

FULL PAPER

Novel nano molten salt tetra-2,3-pyridiniumporphyrinato-oxovanadium tricyanomethanide as a vanadium surface-free phthalocyanine catalyst: Application to Strecker synthesis of α -aminonitrile derivatives

Saeed Baghery¹  | Mohammad Ali Zolfigol¹  | Maliheh Safaiee² | Diego A. Alonso³ | Abbas Khoshnood³

¹Department of Organic Chemistry, Faculty of Chemistry, Bu-Ali Sina University, Hamedan 6517838683, Iran

²Department of Medicinal Plants Production, Nahavand University, Nahavand 6593139565, Iran

³Instituto de Síntesis Orgánica and Departamento de Química Orgánica, Universidad de Alicante, Apdo. 9903080 Alicante, Spain

Correspondence

Saeed Baghery and Mohammad Ali Zolfigol, Department of Organic Chemistry, Faculty of Chemistry, Bu-Ali Sina University, Hamedan 6517838683, Iran.

Email: saadybaghery@yahoo.com; zolfigol@basu.ac.ir; mzolfigol@yahoo.com

Maliheh Safaiee, Department of Medicinal Plants Production, Nahavand University, Nahavand 6593139565, Iran
Email: azalia_s@yahoo.com; msafaiee@nahgu.ac.ir

Diego A. Alonso and Abbas Khoshnood, Instituto de Síntesis Orgánica and Departamento de Química Orgánica, Universidad de Alicante, Apdo. 9903080 Alicante, Spain
Email: diego.alonso@ua.es; abbas.khoshnood@ua.es

Efficient and recyclable novel nano tetra-2,3-pyridiniumporphyrinato-oxovanadium tricyanomethanide, {[VO(TPPA)][C(CN)₃]₄}, as a vanadium surface-free phthalocyanine-based molten salt catalyst was successfully designed, produced and used for the Strecker synthesis of α -aminonitrile derivatives through a one-pot three-component reaction between aromatic aldehydes, trimethylsilyl cyanide and aniline derivatives under neat conditions at 50 °C. This catalyst was well characterized using Fourier transform infrared, UV–visible, X-ray photoelectron and energy-dispersive X-ray spectroscopies, X-ray diffraction, scanning and high-resolution transmission electron microscopies, inductively coupled plasma mass spectrometry and thermogravimetric analysis. The catalyst can be simply recovered and reused several times without significant loss of catalytic activity.

KEYWORDS

molten salt, nano tetra-2,3-pyridiniumporphyrinato-oxo-vanadium tricyanomethanide, phthalocyanine, Strecker synthesis, α -aminonitrile

1 | INTRODUCTION

Metal phthalocyanines are stable and simply attainable macrocyclic complexes employed as cost-effective biomimetic oxidation catalysts and with numerous applications in organic

synthesis.^[1–7] Phthalocyanine derivatives are usually produced via high-temperature cyclotetramerization of phthalic acid or dicyano derivatives.^[8–16] Metal ion templates can significantly increase the yields of these reactions.^[8,10,12,14] Heterocyclic phthalocyanine derivatives containing pyridine,

thionaphthalene, thiophene and pyrazine rings^[17] have also been synthesized and studied in depth. Metal complexes of tetrapyrrolineporphyrins (pyridine derivatives)^[18] are prepared using a template process similar to that of phthalocyanine.^[19–22] Moreover, various syntheses of metallotetrapyrrolineporphyrins by 2,3- and 3,4-pyridinedicarboxylic acid have also been reported.^[23–29]

The Strecker synthesis, firstly reported in 1850,^[30] is the oldest known multicomponent reaction^[30] and the most facile method for the synthesis of α -amino acids on both laboratory and technical scales. The Strecker reaction includes a condensation of an aldehyde with ammonia, in the presence of a cyanide source to form an α -aminonitrile, which is subsequently hydrolysed to the corresponding amino acid.^[30] α -Aminonitriles are popular bifunctional synthons that have found numerous synthetic uses, the most important one being the synthesis of amino acids.^[31] Both these substructures (α -aminonitriles and α -amino acids) are generally synthesized from azomethines via nucleophilic addition reactions, for instance Grignard–Barbier allylations^[32–35] and Strecker-type reactions.^[36–41] The experimental process of the Strecker reaction is tedious, and therefore several modified procedures have been developed using various cyanide reagents (diethylaluminium cyanide, tri-*n*-butyltin cyanide, diethyl phosphorocyanidate and trimethylsilyl cyanide^[42]) and catalysts such as lithium perchlorate,^[43] vanadyl triflate,^[44] zinc halides,^[45] $H_{14}[NaP_5W_{30}O_{110}]$,^[46] montmorillonite KSF^[37] and indium trichloride.^[47]

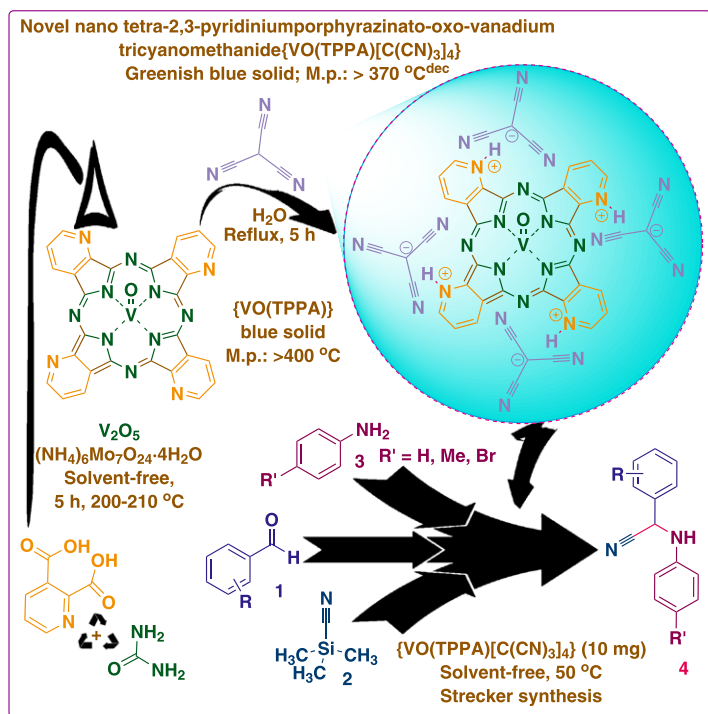
In continuation of our previous studies of the synthesis of novel ionic liquids, molten salts and phthalocyanine-based catalysts and their application in multicomponent

reactions,^[48] herein we introduce nano tetra-2,3-pyridiniumporphyrinato-oxo-vanadium tricyanomethanide, $\{[VO(TPPA)][C(CN)_3]_4\}$, as a vanadium surface-free phthalocyanine-based molten salt catalyst for the Strecker synthesis of α -aminonitrile derivatives by a one-pot three-component reaction of aromatic aldehydes, trimethylsilyl cyanide (TMSCN) and aniline derivatives under neat conditions at 50 °C (Scheme 1).

2 | EXPERIMENTAL

2.1 | General

All chemicals and solvents used were of reagent grade and purchased from Sigma-Aldrich, Fluka, Merck and Acros Organics. All reagents were used without any further purification. TLC analysis was performed on UV-active aluminium-backed F254 silica gel plates. Melting points were measured with a Thermo Scientific apparatus and they were not corrected. Centrifugation procedures were performed with an Anke TDL80-2B. Fourier transform infrared (FT-IR) spectra were recorded with a PerkinElmer FT-IR 17259 spectrometer using KBr discs. UV–visible spectra were recorded with a PerkinElmer 35 UV–visible spectrophotometer. The samples (10 mg) for UV–visible spectral studies were prepared in aqueous ethanol solutions (EtOH–H₂O, 10:1) using a dispersing procedure. ¹H NMR (400 or 300 MHz) spectra were obtained with Bruker Avance 400 and 300 NMR spectrometers, respectively, in proton coupled mode using deuterated dimethylsulfoxide (DMSO) as a solvent, unless otherwise stated. ¹³C NMR (101 MHz) spectra were acquired with a



SCHEME 1 Synthesis of nano tetra-2,3-pyridiniumporphyrinato-oxo-vanadium tricyanomethanide, $\{[VO(TPPA)][C(CN)_3]_4\}$, as a vanadium surface-free phthalocyanine-based molten salt catalyst and its application for the Strecker synthesis of α -aminonitriles

Bruker Avance 400 NMR spectrometer in proton decoupled mode at 20 °C in deuterated DMSO as solvent, unless otherwise stated. Chemical shifts are given in parts per million and the coupling constants (J) in hertz. Data for ^1H NMR are reported as follows: chemical shift (ppm), multiplicity (s, singlet; d, doublet; t, triplet; q, quartet; m, multiplet; and br, broad), coupling constant (Hz) and integration. Thermogravimetric analysis (TGA) was carried out with a Mettler Toledo apparatus (models TGA/SDTA851 and /SF/1100 TG/DTA). TGA was performed under a nitrogen atmosphere at 25 °C and using a heating rate of 20 °C min^{-1} up to 700 °C. High-resolution transmission electron microscopy (HRTEM) images were obtained using a JEOL JEM-2010 microscope operating at an accelerating voltage of 200 kV. Samples were prepared by drop-casting dispersed particles onto a 200-mesh copper grid coated with a holey carbon film. Scanning electron microscopy (SEM) studies were performed using a Hitachi S3000 N, equipped with an X-ray detector (Bruker XFlash 3001) for microanalysis (energy-dispersive X-ray, EDX) and mapping (wavelength-dispersive X-ray, WDX). X-ray diffraction (XRD) analyses were performed using a Bruker D8-Advance apparatus using a monochromatized $\text{Cu K}\alpha$ ($\lambda = 0.154 \text{ nm}$) X-ray source in the range $5^\circ < 2\theta < 60^\circ$. Low-resolution mass spectra (EI) were obtained at 70 eV using an Agilent 5973 Network spectrometer, with fragment ion m/z reported with relative intensities (%) in parentheses. Inductively coupled plasma mass spectrometry (ICP-MS) was performed with an Agilent 7700x apparatus equipped with HMI (high matrix introduction). X-ray photoelectron spectroscopy (XPS; K-ALPHA, Thermo Scientific) was used to analyse sample surfaces. All spectra were collected using

Al-K radiation (1486.6 eV), monochromatized by a twin-crystal monochromator, yielding a focused X-ray spot (elliptical in shape with a major axis length of 400 μm) at 3 mA \times 12 kV. XPS data were analysed using Thermo Scientific Avantage software. A smart background function was used to approximate the experimental backgrounds and surface elemental composition was calculated from background-subtracted peak areas. Charge compensation was achieved with the system flood gun that provides low-energy electrons and low-energy argon ions from a single source.

2.2 | General procedure for synthesis of $\{[\text{VO}(\text{TPPA})][\text{C}(\text{CN})_3]_4\}$

$\{[\text{VO}(\text{TPPA})][\text{C}(\text{CN})_3]_4\}$ was synthesized via the method described by Yokote *et al.*^[25] Urea (13 g), ammonium molybdate $((\text{NH}_4)_6\text{Mo}_7\text{O}_{24}\cdot 4\text{H}_2\text{O}$; 92 mg), 2,3-pyridinedicarboxylic acid (2 g) and vanadium(V) oxide (V_2O_5 ; 200 mg) were ground under neat conditions until a homogeneous mixture was obtained. The mixture was placed in a heating mantle, sealed and heated at 200–210 °C for 5 h. Then, the mixture was allowed to cool to room temperature over a 5 h period. The crude blue solid obtained (8.56 g) was crushed and washed consecutively with warm water, a warm aqueous NaOH solution (5% w/v), warm water, warm diluted aqueous hydrochloric acid (2.5% v/v) and finally with warm water. The obtained crude product was dried at 100 °C under vacuum and finally purified through dissolving in concentrated sulfuric acid and pouring the solution into ice–water. The precipitated product was collected via centrifugation (*ca* 200 rpm/10 min) and transferred to a fine glass sinter funnel where

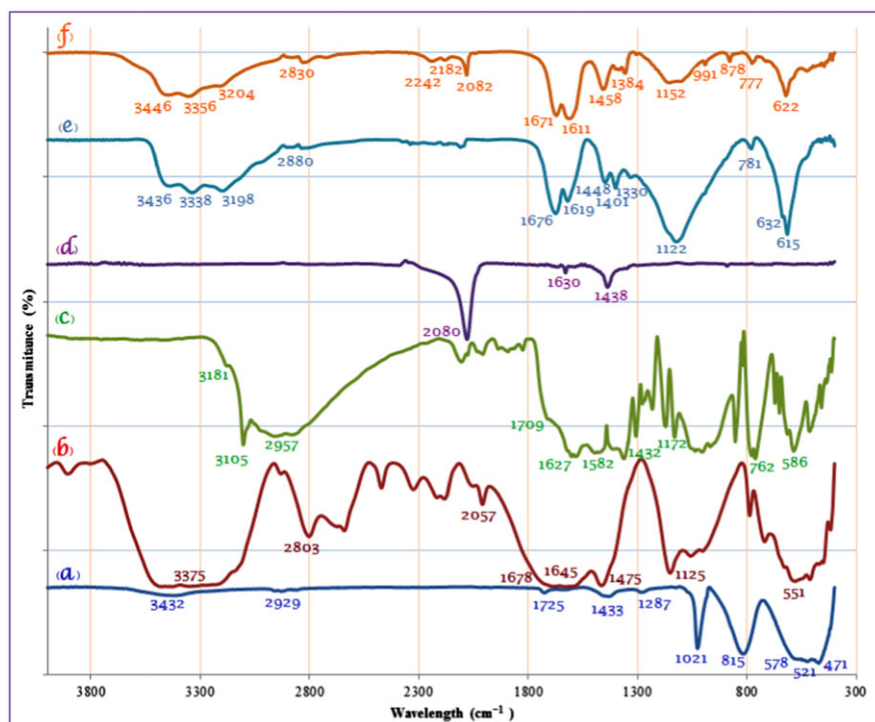


FIGURE 1 FT-IR spectra: (a) V_2O_5 ; (b) urea; (c) 2,3-pyridinedicarboxylic acid; (d) tricyanomethane; (e) $[\text{VO}(\text{TPPA})]$; (f) $\{[\text{VO}(\text{TPPA})][\text{C}(\text{CN})_3]_4\}$

the mass was carefully washed with hot water, a warm aqueous sodium carbonate solution and finally with warm water. [VO(TPPA)] product was dried at 100 °C under vacuum (isolated yield 56%; m.p. > 400 °C) (Scheme 1). The vanadium content of [VO(TPPA)] was measured via ICP-MS, which gave value of about 0.1659% (w/w).

In the next step, to a round-bottomed flask (50 ml) containing a tricyanomethane (4 mmol, 360 mg) aqueous solution (20 ml water), [VO(TPPA)] (1 mmol, 31 mg) was added and stirred over a period of 5 h under reflux conditions. The obtained pale greenish blue solid product {[VO(TPPA)][C(CN)₃]₄} was washed three times with diethyl ether, and then dried under vacuum (isolated yield 93%) (Scheme 1). {[VO(TPPA)][C(CN)₃]₄} (m.p. > 370 °C^{dec}) was fully characterized using FT-IR and UV–visible spectroscopies, XRD, XPS, SEM, HRTEM, EDX, ICP-MS and TGA.

2.3 | General procedure for strecker synthesis of α -aminonitrile derivatives using {[VO(TPPA)][C(CN)₃]₄} as phthalocyanine-based molten salt catalyst

{[VO(TPPA)][C(CN)₃]₄} (10 mg) was added to a mixture of the corresponding aldehyde (1 mmol), TMSCN (1.5 mmol,

149 mg, 188 μ l) and the corresponding aniline derivative (1 mmol). The resulting mixture was stirred at 50 °C under neat conditions and the progress of the reaction was studied using TLC (*n*-hexane–ethyl acetate, 5:2). Once the reaction was finished, the catalyst was filtered and carefully washed with ethanol and then dried under vacuum (the products were soluble in ethanol but {[VO(TPPA)][C(CN)₃]₄} was insoluble). The recycled catalyst was used in the next run of the model reaction. The organic solvent was evaporated and the crude product was purified by a short column of silica gel using (*n*-hexane–ethyl acetate, 20:1) to yield the corresponding pure products.

2.4 | Selected spectral data for compounds

2.4.1 | 2-((4-Bromophenyl)amino)-2-(3,4-dimethoxyphenyl)acetonitrile (4c)

Isolated as yellow solid (305 mg, 88%); m.p. 178–180 °C. FT-IR (KBr, ν , cm⁻¹): 3354, 3011, 2968, 2231, 1593, 1515, 1466, 1265. ¹H NMR (300 MHz, DMSO, δ , ppm): 7.37–7.31 (m, 2H), 7.16–7.09 (m, 2H), 7.04 (d, *J* = 9.0 Hz, 1H), 6.84–6.76 (m, 3H), 5.87 (d, *J* = 9.2 Hz, 1H), 3.78 (2 s, 6H). ¹³C NMR (101 MHz, DMSO, δ , ppm): 149.7, 149.4, 145.8, 132.0, 127.3, 120.1, 119.9, 116.3, 112.2,

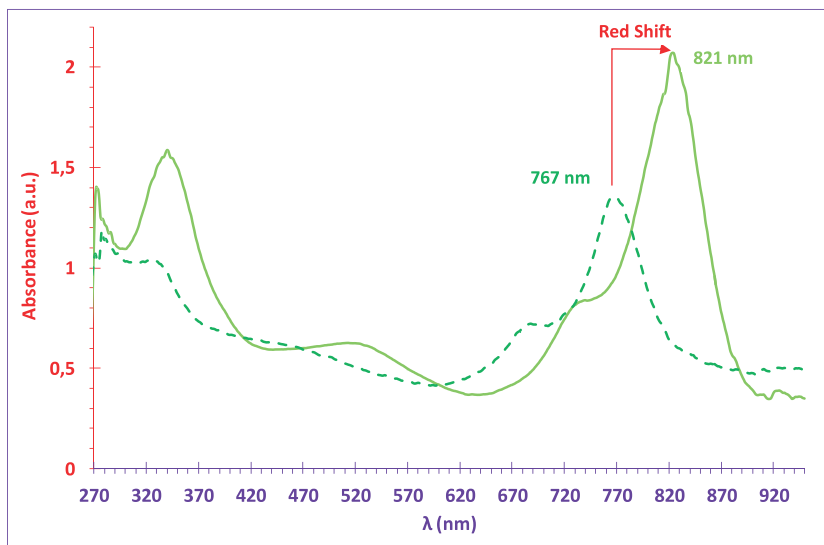


FIGURE 2 UV–visible spectra of {[VO(TPPA)][C(CN)₃]₄} (solid curve) and [VO(TPPA)] (dashed curve)

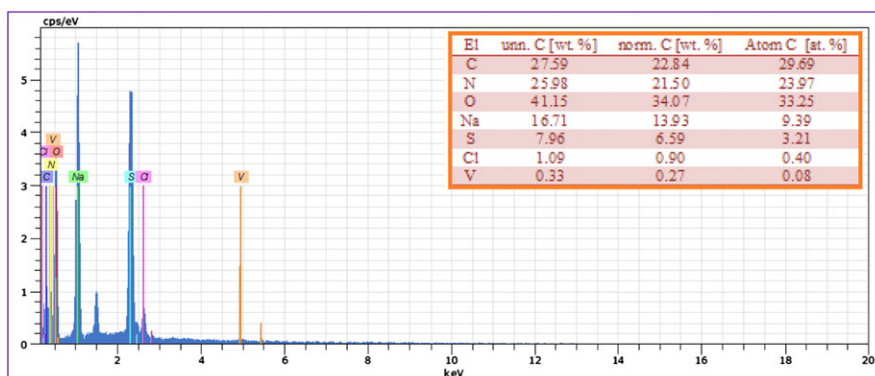


FIGURE 3 EDX spectrum of {[VO(TPPA)][C(CN)₃]₄} as a catalyst

111.3, 109.8, 56.0, 48.3. MS (EI) m/z (%): 346 (M^+ , 100), 320 (21), 218 (24), 207 (14), 179 (12), 176 (54), 165 (17), 157 (10), 155 (10), 78 (22), 76 (10), 63 (26).

2.4.2 | 2-((4-Bromophenyl)amino)-2-(2,5-dimethoxyphenyl)acetonitrile (4e)

Isolated as yellow solid (298 mg, 86%); m.p. 253–255 °C. FT-IR (KBr, ν , cm^{-1}): 3374, 2956, 2234, 1677, 1594, 1499,

1220. ^1H NMR (400 MHz, DMSO, δ , ppm): 7.34–7.28 (m, 2H), 7.11 (d, $J = 3.0$ Hz, 1H), 7.05 (d, $J = 9.0$ Hz, 1H), 6.97 (dd, $J = 9.0, 3.0$ Hz, 1H), 6.80–6.75 (m, 2H), 6.72 (d, $J = 9.2$ Hz, 1H), 5.83 (d, $J = 9.2$ Hz, 1H), 3.79 (s, 3H), 3.71 (s, 3H). ^{13}C NMR (75 MHz, DMSO, δ , ppm): 153.6, 150.9, 145.5, 132.1, 123.4, 119.4, 116.1, 115.2, 114.9, 113.3, 109.9, 56.7, 56.0, 43.8. MS (EI) m/z (%): 346 (M^+ , 8), 335 (12), 174 (40), 165 (100), 78 (13), 63 (18), 44 (14).

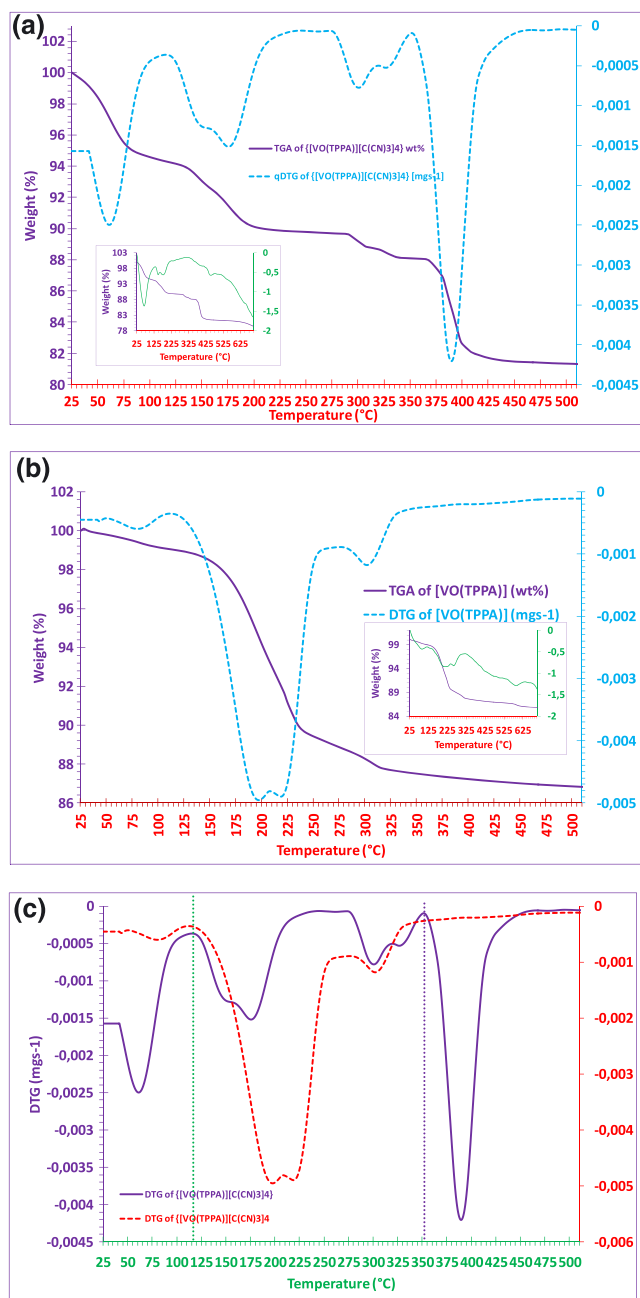


FIGURE 4 (a) TGA/DTG and inlet TGA/DTA of $\{[\text{VO}(\text{TPPA})][\text{C}(\text{CN})_3]_4\}$; (b) TGA/DTG and inlet TGA/DTA of $[\text{VO}(\text{TPPA})]$; (c) comparing superimposed DTG of both $\{[\text{VO}(\text{TPPA})][\text{C}(\text{CN})_3]_4\}$ and $[\text{VO}(\text{TPPA})]$

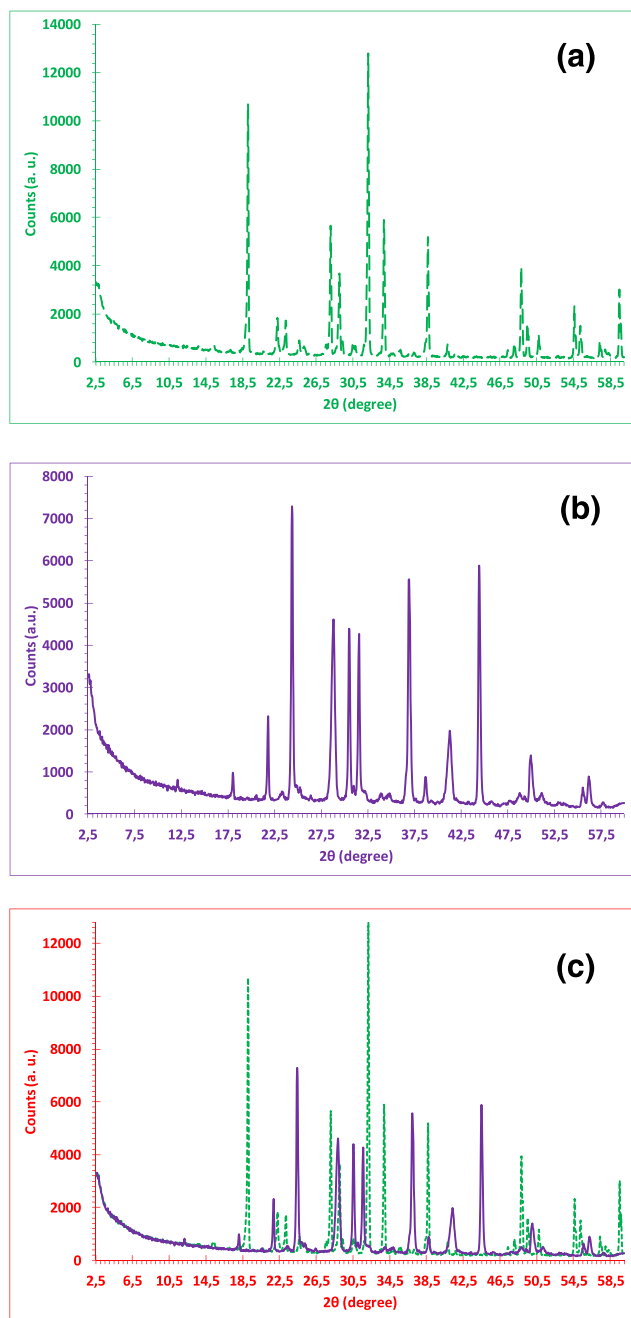


FIGURE 5 XRD patterns: (a) $[\text{VO}(\text{TPPA})]$; (b) $\{[\text{VO}(\text{TPPA})][\text{C}(\text{CN})_3]_4\}$; (c) superimposition of $[\text{VO}(\text{TPPA})]$ (dashed curve) and $\{[\text{VO}(\text{TPPA})][\text{C}(\text{CN})_3]_4\}$ (solid curve)

2.4.3 | 2-((4-Bromophenyl)amino)-2-(naphthalen-1-yl)acetonitrile (4f)

Isolated as yellow solid (303 mg, 90%); m.p. 156–158 °C. FT-IR (KBr, ν , cm^{-1}): 3433, 3293, 3065, 2226, 1653, 1623, 1551, 1497, 1386, 1285. ^1H NMR (300 MHz, DMSO, δ , ppm): 8.11–7.96 (m, 3H), 7.89 (d, $J = 7.0$ Hz, 1H), 7.69–7.56 (m, 3H), 7.39 (d, $J = 9.0$ Hz, 2H), 6.95 (t, $J = 8.5$ Hz, 3H), 6.66 (d, $J = 9.0$ Hz, 1H). ^{13}C NMR (101 MHz, DMSO, δ , ppm): 145.9, 134.0, 132.2, 130.4, 130.3, 130.2, 129.2, 127.4, 126.9, 126.2, 125.8, 123.8, 119.6, 116.0, 109.8, 47.1. MS (EI) m/z (%): 336 (M^+ , 26), 310 (16), 166 (100), 127 (10), 127 (10).

2.4.4 | 2-([1,1'-biphenyl]-4-yl)-2-((4-bromophenyl)amino)acetonitrile (4g)

Isolated as yellow solid (330 mg, 91%); m.p. 151–153 °C. FT-IR (KBr, ν , cm^{-1}): 3306, 3064, 2216, 1634, 1605, 1578, 1547, 1384, 1302, 1184. ^1H NMR (300 MHz, DMSO, δ , ppm): 7.80–7.75 (m, 2H), 7.71–7.61 (m, 4H), 7.56–7.43 (m, 3H), 7.36–7.31 (m, 2H), 6.96 (d, $J = 9.2$ Hz, 1H), 6.88–6.74 (m, 2H), 6.06 (d, $J = 9.2$ Hz, 1H). ^{13}C NMR (75 MHz, DMSO, δ , ppm): 145.7, 141.2, 134.2, 132.1, 131.9, 129.5, 128.3, 127.7, 127.2, 127.1, 122.7, 116.3, 109.9, 48.4. MS (EI) m/z (%): 362 (M^+ , 72), 351 (12), 334 (16), 281 (23), 181 (100), 152 (51).

2.4.5 | 2-((4-Bromophenyl)amino)-2-(4-methoxyphenyl)acetonitrile (4i)

Isolated as yellow solid (282 mg, 89%); m.p. 146–148 °C. FT-IR (KBr, ν , cm^{-1}): 3435, 3092, 2191, 1633, 1588,

1553, 1495, 1384, 1228. ^1H NMR (300 MHz, CDCl_3 , δ , ppm): 7.54–7.45 (m, 2H), 7.40–7.32 (m, 2H), 7.02–6.92 (m, 2H), 6.70–6.61 (m, 2H), 5.32 (d, $J = 8.1$ Hz, 1H), 4.02 (d, $J = 8.1$ Hz, 1H), 3.84 (s, 3H). ^{13}C NMR (75 MHz, DMSO, δ , ppm): 160.1, 145.8, 132.0, 129.1, 127.0, 119.9, 116.3, 114.8, 109.7, 55.7, 48.1. MS (EI) m/z (%): 316 (M^+ , 30), 290 (29), 146 (100), 63 (10).

2.4.6 | 2-((4-Bromophenyl)amino)-2-(naphthalen-2-yl)acetonitrile (4j)

Isolated as yellow solid (303 mg, 90%); m.p. 263–265 °C. FT-IR (KBr, ν , cm^{-1}): 3547, 3475, 3413, 3233, 3058, 2242, 1638, 1618, 1488, 1384, 1105. ^1H NMR (300 MHz, DMSO, δ , ppm): 8.13 (s, 1H), 8.06–7.95 (m, 3H), 7.66 (dd, $J = 9.0$, 1.8 Hz, 1H), 7.62–7.55 (m, 2H), 7.38–7.32 (m, 2H), 7.03 (d, $J = 9.2$ Hz, 1H), 6.90–6.77 (m, 2H), 6.21 (d, $J = 9.2$ Hz, 1H). ^{13}C NMR (101 MHz, DMSO, δ , ppm): 145.8, 133.3, 133.1, 132.6, 132.1, 129.3, 128.5, 128.1, 127.3 (2c), 126.6, 125.3, 119.6, 116.3, 109.9, 48.8. MS (EI) m/z (%): 336 (M^+ + 2, 11), 334 (M^+ , 11), 327 (14), 155 (100), 127 (51).

2.4.7 | 2,2'-(1,4-phenylene)bis(2-((4-bromophenyl)amino)acetonitrile) (4k)

Isolated as yellow solid (446 mg, 90%); m.p. 194–196 °C. FT-IR (KBr, ν , cm^{-1}): 3377, 3347, 2182, 1593, 1492, 1397, 1297, 1071. ^1H NMR (400 MHz, DMSO, δ , ppm): 7.67 (s, 4H), 7.37–7.32 (m, 4H), 6.96 (dd, $J = 9.3$, 2.1 Hz, 2H), 6.81–6.77 (m, 4H), 6.08 (d, $J = 8.8$ Hz, 2H). ^{13}C NMR (101 MHz, DMSO, δ , ppm): 145.6, 135.9, 132.1, 128.4, 119.5, 116.3, 110.0, 48.3. MS (EI) m/z (%): 495 (M

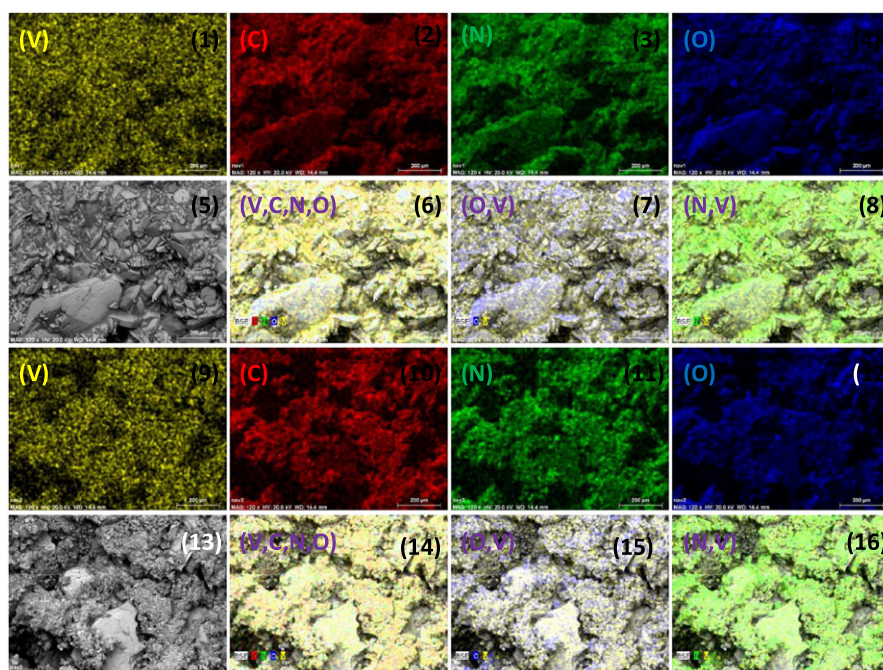


FIGURE 6 SEM images and WDX elemental maps of [VO(TPPA)] (1–8) and {[VO(TPPA)][C(CN)₃]₄} (9–16)

⁺, 3), 492 (20), 467 (100), 442 (97), 299 (11), 286 (13), 259 (12), 182 (17), 155 (59), 116 (14), 76 (29).

3 | RESULTS AND DISCUSSION

3.1 | Characterization of {[VO(TPPA)][C(CN)₃]₄} as Phthalocyanine-Based Molten Salt Catalyst

Catalyst {[VO(TPPA)][C(CN)₃]₄} was synthesized via the method described by Yokote *et al.* using urea, tetrahydrated ammonium molybdate ((NH₄)₆Mo₇O₂₄·4H₂O), 2,3-pyridinedicarboxylic acid and vanadium(V) oxide.^[25] The structure of {[VO(TPPA)][C(CN)₃]₄} was investigated and fully characterized via FT-IR and UV-visible spectroscopies, XRD, XPS, SEM, HRTEM, EDX, ICP-MS and TGA.

In the FT-IR spectrum of {[VO(TPPA)][C(CN)₃]₄}, the absorption bands at 991 and 622 cm⁻¹ are related to the stretching vibrational modes of V=O. Additionally, the absorption bands at 1611 cm⁻¹ (linked to C=N stretching) and at 1458 cm⁻¹ (related to C=C stretching) are also observed in the FT-IR spectrum of the catalyst. The known peaks at 2242, 2182 and 2082 cm⁻¹ are linked to C≡N stretching on tricyanomethanide counter ion. Also, the identified peaks at 3446, 3356 and 3204 cm⁻¹ are assigned to the N-H stretching absorptions of the pyridinium ring. A comparison of the FT-IR spectrum of catalyst {[VO(TPPA)][C(CN)₃]₄} with those of other substrates and [VO(TPPA)] is presented in Figure 1.

The structure of {[VO(TPPA)][C(CN)₃]₄} was also studied and compared with that of [VO(TPPA)] using UV-visible spectroscopy. Thus, aqueous ethanol solutions (EtOH-H₂O, 10:1) of {[VO(TPPA)][C(CN)₃]₄} and [VO(TPPA)] were prepared and analysed. As depicted in Figure 2, these compounds show strong absorption bands at 821 and 767 nm (visible region), respectively. Furthermore, the optical bandgap energies ($E_{bg} = 1240/\lambda_{max}$) for {[VO(TPPA)][C(CN)₃]₄} and [VO(TPPA)] were calculated, resulting 1.510 and 1.616 eV, respectively. It is important to underline that while synthesizing {[VO(TPPA)][C(CN)₃]₄}, the colour of the aqueous reaction solution changed from green to pale green while adding tricyanomethanide counter ion (see Section 1). This acid-base behaviour mechanism is found to be similar in UV-visible analysis. Thus, the red-shift differences in the absorption maximum between the catalyst and [VO(TPPA)] can be considered as proof of the formation of the catalyst.

The metallic composition of {[VO(TPPA)][C(CN)₃]₄} and [VO(TPPA)] was determined using EDX, ICP-MS and TGA.

The EDX data obtained for {[VO(TPPA)][C(CN)₃]₄} confirm the presence of the anticipated elements in the structure of the catalyst: carbon, nitrogen, oxygen and vanadium (Figure 3). No extra peaks connected with any impurity are

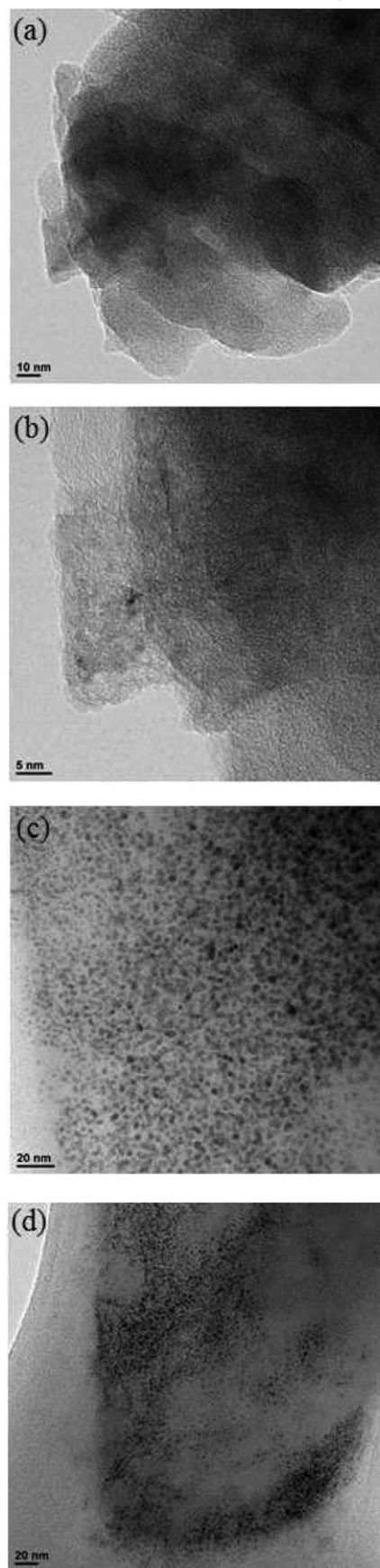


FIGURE 7 HRTEM images of (a, b) [VO(TPPA)] and (c, d) {[VO(TPPA)][C(CN)₃]₄}

detected in SEM-coupled EDX analysis, confirming the catalyst composition: C (22.84%), N (21.50%), O (34.07%) and V (0.27%). Moreover, a catalyst vanadium content of 0.08112% (*w/w*) was determined using ICP-MS. In addition, the vanadium content of [VO(TPPA)] was measured via ICP-MS, which gives a value of 0.1659% (*w/w*).

Figure 4 shows the thermal behaviour of {[VO(TPPA)][C(CN)₃]₄} and [VO(TPPA)] under nitrogen atmosphere. TGA, derivative thermogravimetric analysis (DTG) and differential

thermal analysis (DTA) of the catalyst were generally investigated.

The DTA diagram shows a general negative downward slope between 25 and 700 °C in which decomposition of catalyst and its precursor in nitrogen atmosphere is exothermic. Moreover, the TGA, DTG and DTA thermal decomposition processes, as shown in Figure 4(a–c), include three steps. The first one, related to the removal of surface-adsorbed water and organic solvents, takes place between 25 and

TABLE 1 XRD data for {[VO(TPPA)][C(CN)₃]₄}

Entry	2θ (°)	Peak width, FWHM (°)	Size (nm)	Inter-planar distance (nm)
1	18.05	0.34	23.66	0.490868
2	21.85	0.25	32.37	0.406172
3	24.40	0.27	30.11	0.364368
4	28.85	0.45	18.23	0.309098
5	30.50	0.22	37.43	0.292741
6	31.60	0.20	41.28	0.282797
7	36.90	0.27	31.02	0.243304
8	38.70	0.36	23.39	0.232391
9	41.30	0.59	14.39	0.218342
10	44.45	0.26	33.01	0.203572
11	49.90	0.44	19.91	0.182539
12	55.55	0.41	21.90	0.165236
13	56.20	0.39	23.10	0.163478

TABLE 2 XRD data for [VO(TPPA)]

Entry	2θ (°)	Peak width, FWHM (°)	Size (nm)	Inter-planar distance (nm)
1	19.05	0.15	53.70	0.465319
2	22.25	0.23	35.21	0.399067
3	23.15	0.23	35.26	0.383753
4	28.05	0.17	48.25	0.317729
5	29.00	0.20	41.03	0.307533
6	32.15	0.10	82.81	0.278084
7	33.90	0.21	39.56	0.264117
8	38.65	0.18	46.78	0.232680
9	48.80	0.24	36.35	0.186394
10	49.45	0.24	36.44	0.184095
11	50.80	0.25	35.17	0.179845
12	54.60	0.14	63.87	0.167884
13	55.20	0.29	30.91	0.166200
14	59.50	0.14	65.37	0.155174
15	59.55	0.31	29.53	0.155056

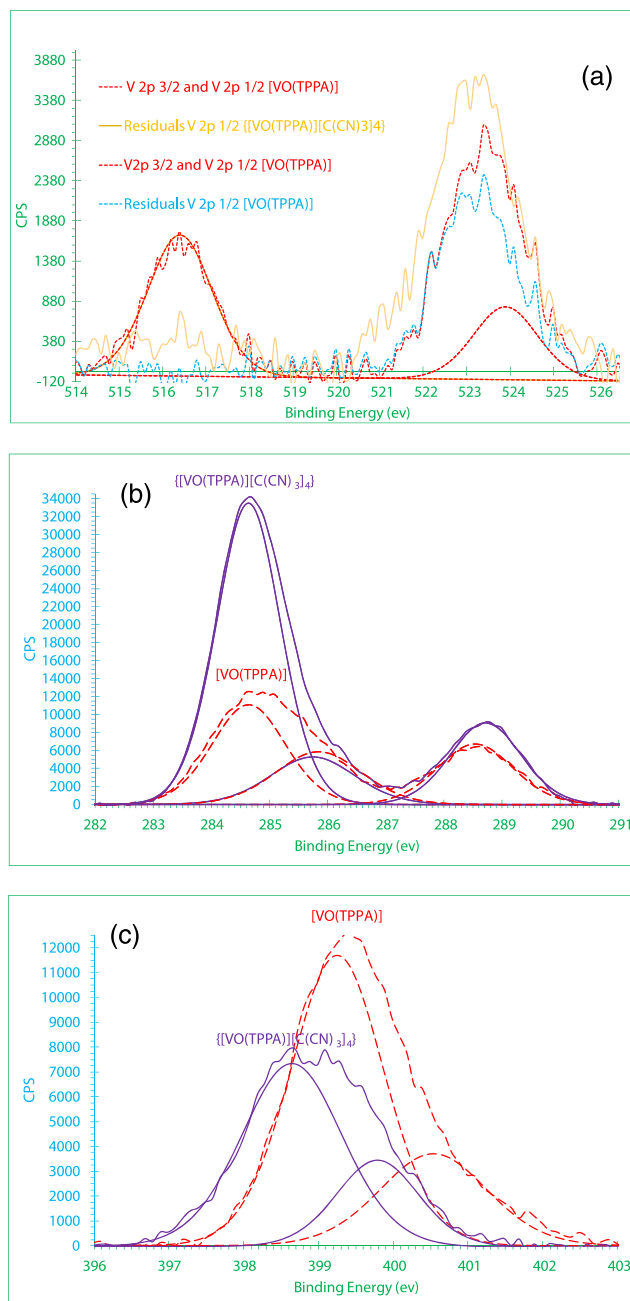


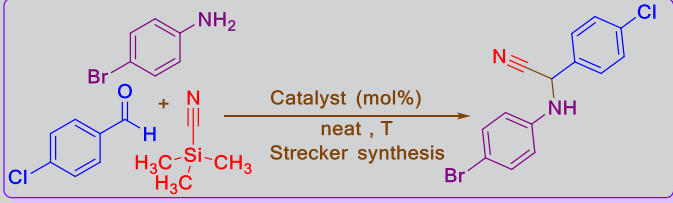
FIGURE 8 High-resolution XPS spectra: (a) V 2p in [VO(TPPA)] (red lines with blue residuals lines) and in {[VO(TPPA)][C(CN)₃]₄} (orange residuals lines); (b) C 1s in [VO(TPPA)] (dashed curves) and in {[VO(TPPA)][C(CN)₃]₄} (solid curves); (c) N 1s in [VO(TPPA)] (dashed curves) and in {[VO(TPPA)][C(CN)₃]₄} (solid curves)

110 °C and involves a weight loss of 0.9 and 5.6% for [VO(TPPA)] and {[VO(TPPA)][C(CN)₃]₄}, respectively. The higher percentage of absorbed water for catalyst when compared with its precursor can be reasoned for the ionic molten salt nature of {[VO(TPPA)][C(CN)₃]₄}. The second weight loss region shown between 110 and 405 °C is attributed to the continuing decomposition of the phthalocyanine ring. Weight losses of 10.2 and 4.7 wt% are observed for [VO(TPPA)] for {[VO(TPPA)][C(CN)₃]₄}, respectively. Finally, the third weight loss region for {[VO(TPPA)][C(CN)₃]₄} (between 405 and 510 °C) can be ascribed to the continuing decomposition of the ionic (pyridinium/tricyanomethanide) moieties of the catalyst. On the contrary, no distinct weight loss is detected in this temperature range for [VO(TPPA)], suggesting a non-ionic nature of this material. The weight loss for this third step is calculated to be lower than 0.1% for [VO(TPPA)] and 8.5% for {[VO(TPPA)][C(CN)₃]₄}. In

addition, above 700 °C, no significant weight loss is observed. As clearly indicated in Figure 4(c) for the results of the DTG analysis, the thermal stability of the catalyst is improved from 110–405 to 405–510 °C when compared with its precursor, which can be attributed to the ionic character of the pyridinium functional groups.

The particle size and shape as well as the morphology of {[VO(TPPA)][C(CN)₃]₄} and [VO(TPPA)] were studied using XRD, SEM and HRTEM (Figures 5–7). Characterization by XRD was performed to investigate the crystalline structure of {[VO(TPPA)][C(CN)₃]₄} and [VO(TPPA)] in the range $2\theta = 2.5\text{--}60^\circ$ (Figure 5). The XRD analysis reveals 13 characteristic peaks for the catalyst between 18.05° and 56.20° . The peak width (FWHM), size and inter-planar distance from the XRD pattern of the catalyst were studied and the results are summarized in Table 1. A similar analysis for [VO(TPPA)] is summarized in Table 2. These

TABLE 3 Reaction conditions optimization of Strecker synthesis under neat conditions^a



Entry	Catalyst	Catalyst loading (Mol%)	Reaction temperature (°C)	Time (min)	Yield (%) ^b
1	{[Vo(TPPA)][C(CN) ₃] ₄ }	0.016	50	20	91
2	[Msim]Cl	2	50	30	85
3	NH ₂ SO ₃ H	10	50	45	—
4	[MIMPS] ₃ PW ₁₂ O ₄₀	2	50	30	87
5	H ₃ PW ₁₂ O ₄₀	5	50	30	78
6	Acetic acid	20	50	45	53
7	[Dsim]Cl	2	50	30	85
8	Ce(HSO ₄) ₃ ·7H ₂ O	20	50	45	—
9	[TEAPS] ₃ PW ₁₂ O ₄₀	2	50	30	85
10	HBF ₄	10	50	30	61
11	{[Vo(TPPA)][C(CN) ₃] ₄ }	0.008	50	30	75
12	{[Vo(TPPA)][C(CN) ₃] ₄ }	0.032	50	20	91
13	{[Vo(TPPA)][C(CN) ₃] ₄ }	0.08	50	20	88
14	{[Vo(TPPA)][C(CN) ₃] ₄ }	0.16	50	20	85
15	Catalyst-free	—	50	60	—
16	{[Vo(TPPA)][C(CN) ₃] ₄ }	0.016	r.t.	30	57
17	{[Vo(TPPA)][C(CN) ₃] ₄ }	0.016	75	20	91
18	{[Vo(TPPA)][C(CN) ₃] ₄ }	0.016	100	20	91
19	[Vo(TPPA)]	0.032	50	30	88
20	NaCl	0.5	50	60	—

^aReaction conditions: 4-chlorobenzaldehyde (1 mmol, 140 mg), TMSCN (1.5 mmol, 149 mg, 188 μ l), 4-bromoaniline (1 mmol, 172 mg).

^bIsolated yield.

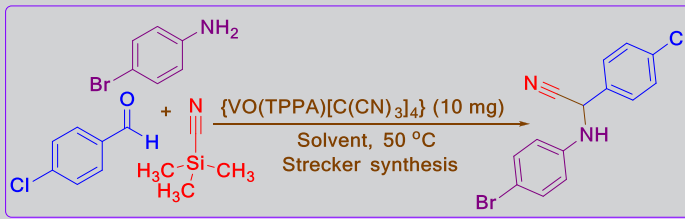
characteristic peaks indicate crystallographic planes of the catalyst. The broad peak ($2\theta = 24.40^\circ$) represents nanometre-sized crystallites. In addition the average crystalline size D (nm) of the catalyst can be estimated according to the Scherrer equation: $D = K\lambda/(\beta\cos\theta)$. The calculated average particle sizes for $\{[\text{VO}(\text{TPPA})][\text{C}(\text{CN})_3]_4\}$ and $[\text{VO}(\text{TPPA})]$ are summarized in Tables 1 and 2, respectively. On the other hand, the average inter-planar distance (nm) of $\{[\text{VO}(\text{TPPA})][\text{C}(\text{CN})_3]_4\}$ and $[\text{VO}(\text{TPPA})]$ were calculated according to the Bragg equation: $d_{hkl} = \lambda/(2\sin\theta)$. Moreover, the crystalline diffraction lines of $\{[\text{VO}(\text{TPPA})][\text{C}(\text{CN})_3]_4\}$ show different angle from those of $[\text{VO}(\text{TPPA})]$, as depicted in Figure 5(c), where the superimposed XRD patterns of both materials are shown. Also, the XRD pattern changes of $\{[\text{VO}(\text{TPPA})][\text{C}(\text{CN})_3]_4\}$ catalyst in comparison with $[\text{VO}(\text{TPPA})]$ indicate the production of the catalyst (Figure 5).

The surface texture and morphological properties of the catalyst were also studied using SEM (Figure 6) and HRTEM (Figure 7). Both analyses show that the catalyst morphology is fibrillar and with suitable monodispersity. The catalyst synthesis employed in this investigation produces a uniform dispersion of small particles with average size of 14.39–41.28 nm, which is in accordance with the XRD results. Moreover, in combination with SEM, WDX provides qualitative information about the distribution of various chemical elements in the catalyst matrix. Figure 6 collects representative SEM images and WDX elemental maps for the produced catalyst. It can be seen that vanadium metal particles are finely dispersed in the material. The selected-area elemental analysis

indicates the presence of C, N, O and V, which proves the regular uniformity of the synthesized catalyst.

XPS studies were next performed of $\{[\text{VO}(\text{TPPA})][\text{C}(\text{CN})_3]_4\}$ and $[\text{VO}(\text{TPPA})]$ in order to obtain an insight into the surface composition of these materials. As depicted in Figure 8(a) for $[\text{VO}(\text{TPPA})]$ (red and blue lines), the V 2p peaks can be fitted into the two different peaks located at 516.39 and 523.89 eV (in red) corresponding to $2p_{3/2}$ and $2p_{1/2}$ levels with a relative area of 1 to 0.52, respectively, with a blue residuals lines located at 523.48 eV. On the other hand, for $\{[\text{VO}(\text{TPPA})][\text{C}(\text{CN})_3]_4\}$ (Figure 8a, orange lines), the peaks for vanadium $2p_{3/2}$ and $2p_{1/2}$ are not detected, and only orange residuals lines located at 522.68 eV is observed. Since the ICP-MS, EDX and elemental mapping analyses had previously indicated the presence of vanadium in both $\{[\text{VO}(\text{TPPA})][\text{C}(\text{CN})_3]_4\}$ and $[\text{VO}(\text{TPPA})]$, this result suggests the absence of vanadium oxide on the surface of the catalyst.^[49] Moreover, the C 1s XPS spectrum of $[\text{VO}(\text{TPPA})]$ (Figure 8b, red lines) can be deconvoluted into three peaks at 286.64, 285.74 and 288.54 eV, revealing the existence of C=C, C=N and N=C=N moieties, respectively (ratio of 1:0.55:0.63). However, compared with $[\text{VO}(\text{TPPA})]$, the binding energy of C=N and N=C=N of $\{[\text{VO}(\text{TPPA})][\text{C}(\text{CN})_3]_4\}$ shifts to 285.84 and 288.71 eV. This positive shift of the binding energy suggests the presence of pyridinium NH^+ moieties. In addition, Figure 8(a,b) also shows the reduction of the C=N (0.55 to 0.23) and N=C=N (0.63 to 0.30) functional groups in the catalyst when compared with the precursor.

TABLE 4 $\{[\text{VO}(\text{TPPA})][\text{C}(\text{CN})_3]_4\}$ -catalysed Strecker reaction: solvent optimization^a



Entry	Solvent	Time (min)	Yield (%) ^b
1	H ₂ O	30	84
2	C ₂ H ₅ OH	30	87
3	CH ₃ CN	30	81
4	CH ₃ CO ₂ Et	45	75
5 ^c	CH ₂ Cl ₂	45	68
6	Toluene	60	51
7	<i>n</i> -hexane	60	45
8	Neat	20	91

^aReaction conditions: 4-chlorobenzaldehyde (1 mmol, 140 mg), TMSCN (1.5 mmol, 149 mg, 188 μ l), 4-bromoaniline (1 mmol, 172 mg).

^bIsolated yield.

^cReaction in CH₂Cl₂ as a solvent was investigated under reflux condition.

3.2 | Application of {[VO(TPPA)][C(CN)₃]₄} as phthalocyanine-based molten salt catalyst for strecker synthesis of α -aminonitriles

In continuation of our studies^[48] related to the applications of {[VO(TPPA)][C(CN)₃]₄} in organic synthesis, we next studied the use of this catalyst in the Strecker synthesis of α -aminonitriles (Scheme 1). To find simple and appropriate conditions for the Strecker synthesis of α -aminonitriles, we performed the corresponding optimization for a model reaction between 4-chlorobenzaldehyde (1 eq.) and 4-bromoaniline (1 eq.) in the presence of TMSCN (1.5 eq.).

To optimize the reaction conditions, the reaction was studied using various catalysts under neat conditions. The use of 50 mg of {[VO(TPPA)][C(CN)₃]₄} under these

conditions provides an 88% yield (Table 3, entry 13) of the desired product. Optimization of the reaction conditions was undertaken to increase the yield employing various amounts of catalyst. The yield is increased to 91% using 10 or 20 mg of catalyst (Table 3, entries 1 and 12). However, the addition of 100 mg of the catalyst is found to have an inhibitory effect on the production of α -aminonitriles (Table 3, entry 14), while a reduction in yield is observed by decreasing the catalyst loading to 5 mg (Table 3, entry 11). The influence of other catalysts was also examined. With NH₂SO₃H, Ce(HSO₄)₃·7H₂O and NaCl the reaction does not proceed (Table 3, entries 3, 8 and 20) and with other catalysts the isolated yield of desired product is appropriately obtained. The results achieved with other catalysts are summarized in Table 3. Also, for the model reaction in the

TABLE 5 Strecker synthesis of α -aminonitrile derivatives in the presence of 10 mg of {[VO(TPPA)][C(CN)₃]₄} as phthalocyanine-based molten salt catalyst under solvent-free conditions at 50 °C^a

Entry	Aldehyde	Aniline	M.p. (°C)	Time (min)	Yield (%) ^b	TOF
4a	4-Chlorobenzaldehyde	4-Bromoaniline	337–339 (yellow solid) ^[50]	20	91	284.38
4b	4-Nitrobenzaldehyde	Aniline	33–35 (red solid) ^[51]	25	90	225.00
4c	3,4-Dimethoxybenzaldehyde	4-Bromoaniline	178–180 (yellow solid)	30	88	183.33
4d	4-Nitrobenzaldehyde	4-Bromoaniline	303–305 (orange solid) ^[50]	15	93	387.50
4e	2,5-Dimethoxybenzaldehyde	4-Bromoaniline	253–255 (yellow solid)	30	86	179.17
4f	Naphthalene-1-carbaldehyde	4-Bromoaniline	156–158 (yellow solid)	25	90	225.00
4g	Biphenyl-4-carbaldehyde	4-Bromoaniline	151–153 (yellow solid)	25	91	227.50
4h	4-Nitrobenzaldehyde	4-methylaniline	87–89 (red solid) ^[51]	20	91	284.38
4i	4-Methoxybenzaldehyde	4-Bromoaniline	146–148 (yellow solid)	30	89	185.42
4j	Naphthalene-2-carbaldehyde	4-Bromoaniline	263–265 (yellow solid)	25	90	225.00
4k	4-Chlorobenzaldehyde	Aniline	110–112 (brown solid) ^[51]	30	87	181.25
4l	4-Chlorobenzaldehyde	4-methylaniline	87–89 (brown solid) ^[52]	25	89	222.50
4m	4-Methylbenzaldehyde	Aniline	73–75 (green solid) ^[51]	40	85	132.81
4n	4-Methylbenzaldehyde	4-methylaniline	105–107 (green solid) ^[51]	35	87	155.36
4o	Terephthaldehyde	Aniline	161–163 (yellow solid) ^[53]	30	88	183.33
4p	4-Dimethylaminobenzaldehyde	Aniline	105–107 (red solid) ^[54]	35	86	153.57
4q	Terephthaldehyde	4-Bromoaniline	194–196 (yellow solid)	25	90	225.00
4r	4-Methylbenzaldehyde	4-Bromoaniline	218–220 (yellow solid) ^[54]	30	89	185.42
4s	Benzaldehyde	Aniline	83–85 (green solid) ^[51]	45	85	118.06
4t	Benzaldehyde	4-methylaniline	106–108 (green solid) ^[51]	40	87	135.94

^aReaction conditions: aldehyde (1 mmol), TMSCN (1.5 mmol, 149 mg, 188 μ l), aniline derivatives (1 mmol).

^bIsolated yield.

absence of catalyst the desired product is not obtained (Table 3, entry 15). Other catalysts are not efficient under similar conditions, and therefore $\{[\text{VO}(\text{TPPA})][\text{C}(\text{CN})_3]_4\}$ was chosen as the best catalyst. Next, the effect of temperature on the rate of reaction was investigated. When the reaction is performed at 50 °C, the maximum yield is obtained in a short reaction time (Table 3, entry 1). Furthermore, increasing the temperature to more than 50 °C has no change on the yield or reaction time (Table 3, entries 17 and 18). Also, it is found that, at room temperature, the reaction is very slow and does not progress to completion (Table 3, entry 16).

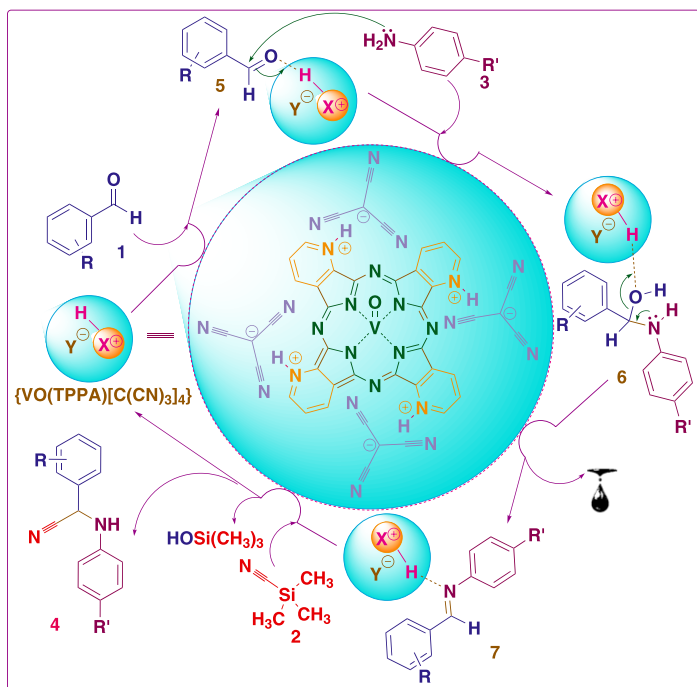
Next, we carried out an optimization of the reaction media (Table 4). Generally, polar solvents lead to higher yields than non-polar ones. However, as evident from entries 1–7, the use of solvent is detrimental for the reaction yield. Finally, it is evident that neat conditions afford the best result in terms of reaction time and yield (Table 4, entry 8) probably due to a more intimate contact between the reactants and the catalyst surface under these conditions.

To study the versatility and generality of the optimized process, the reaction was extended to various aromatic aldehydes. The results are summarized in Table 5. It is obvious that the product yield is influenced by both electronic and steric effects of the substituted groups. Aromatic aldehydes with electron-donating groups give lower yields than those bearing electron-withdrawing substituents. Additionally, the effect of steric hindrance on the aromatic aldehydes is important. In general, *ortho*-substituted aromatic aldehydes provide lower yields. On the other hand, hetero-aromatic aldehydes require longer reaction times than aromatic aldehydes affording lower yields as well. The structures of

α -aminonitriles were determined from ^1H NMR, ^{13}C NMR, GC–MS and FT-IR spectral data. In order to evaluate the efficacy of $\{[\text{VO}(\text{TPPA})][\text{C}(\text{CN})_3]_4\}$ as a catalyst for the Strecker synthesis of α -aminonitrile derivatives, turnover frequency (TOF) values were also calculated (according to the ICP-MS results, 10 mg of catalyst is equivalent to 0.016 mol% of catalyst). Furthermore, for this reaction condition 4-bromoaniline reacts faster than 4-methylaniline and aniline. Moreover, in the presence of terephthalaldehyde as an aldehyde derivative, α -bisaminonitrile products are obtained (Table 5, entries 15 and 17). No by-products from the cyanide addition to the aldehydes are detected in the crude reaction mixtures due to the rapid activation of the *in situ* produced imine by the catalyst.^[51,55,56]

According to previous studies,^[51,55,56] we present a plausible pathway for the Strecker synthesis of α -aminonitriles in the presence of $\{[\text{VO}(\text{TPPA})][\text{C}(\text{CN})_3]_4\}$ as a vanadium surface-free phthalocyanine-based molten salt catalyst in Scheme 2. Thus, in the absence of vanadium oxide in the surface of the catalyst, the pyridinium NH^+ moieties of $\{[\text{VO}(\text{TPPA})][\text{C}(\text{CN})_3]_4\}$ activate the carbonyl group of the aromatic aldehydes **1** via hydrogen bonding towards nucleophilic attack of the aniline derivatives **3**. This reaction would produce the corresponding imines **7**, a process promoted by the water physically and/or chemically adsorbed on the catalyst surface. In the next step, a similar catalyst hydrogen-bonding activation on both the generated imine **7** and TMSiCN (by generation of pentacoordinated Si) takes place affording the corresponding α -aminonitriles **4** and trimethylsilanol (Scheme 2).

The recyclability of the catalyst was also investigated by running seven consecutive cycles of the model synthesis of



SCHEME 2 Plausible mechanism for Strecker synthesis of α -aminonitriles using $\{[\text{VO}(\text{TPPA})][\text{C}(\text{CN})_3]_4\}$ as a phthalocyanine-based molten salt catalyst

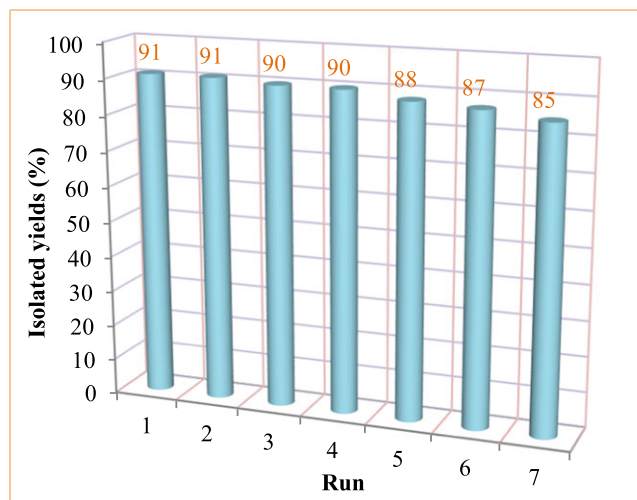


FIGURE 9 Reusability studies of $\{[\text{VO}(\text{TPPA})][\text{C}(\text{CN})_3]_4\}$ as phthalocyanine-based molten salt catalyst for Strecker synthesis of α -aminonitrile 4a

4a. It is important to underline that the reaction product can be simply separated from the catalyst based on solubility issues (see Section 1). Then, after each run, the catalyst was filtered, exhaustively washed with ethanol (where the products are soluble but not the catalyst) and finally dried. As seen in Figure 9, the $\{[\text{VO}(\text{TPPA})][\text{C}(\text{CN})_3]_4\}$ catalyst promotes the reactions without significant loss of catalytic activity. FT-IR analysis of $\{[\text{VO}(\text{TPPA})][\text{C}(\text{CN})_3]_4\}$ after the seventh run confirms the stability of the nanocatalyst during the recycling procedure.

4 | CONCLUSIONS

We have synthesized and fully characterized (FT-IR and UV-visible spectroscopies, XRD, XPS, SEM, HRTEM, EDX, ICP-MS and TGA) nano tetra-2,3-pyridiniumporphyrinato-oxo-vanadium tricyanomethanide, $\{[\text{VO}(\text{TPPA})][\text{C}(\text{CN})_3]_4\}$, as a vanadium surface-free phthalocyanine-based molten salt which is an efficient and recyclable catalyst for the Strecker synthesis of α -aminonitriles. The reported one-pot synthesis of α -aminonitriles is a suitable alternative to multi-step methodologies and offers various advantages, such as wide functional group tolerance, high reaction rates and yields, neat conditions and use of a stable and recyclable catalyst.

ACKNOWLEDGMENTS

We thank Bu-Ali Sina University, Nahavand University, the Iran National Science Foundation (INSF, grant no. 95820271), the National Elites Foundation, the University of Alicante (VIGROB-173) and the Spanish Ministerio de

Economía y Competitividad (CTQ2015-66624-P) for financial support to our research groups.

REFERENCES

- [1] C. Pérollier, A. B. Sorokin, *Chem. Commun.* **2002**, 1548.
- [2] B. Meunier, A. Sorokin, *Acc. Chem. Res.* **1997**, *30*, 470.
- [3] A. Sorokin, S. De Suzzoni-Dezard, D. Poullain, J. P. Noel, B. Meunier, *J. Am. Chem. Soc.* **1996**, *118*, 7410.
- [4] A. Hadasch, A. Sorokin, A. Rabion, L. Fraisse, B. Meunier, *Bull. Soc. Chim. Fr.* **1997**, *134*, 1025.
- [5] A. Sorokin, B. Meunier, *J. Chem. Soc. Chem. Commun.* **1799**, 1994.
- [6] A. Sorokin, J. L. Seris, B. Meunier, *Science* **1995**, *268*, 1163.
- [7] K. Kasuga, K. Mori, T. Sugimori, M. Handa, *Bull. Chem. Soc. Jpn.* **2000**, *73*, 939.
- [8] C. C. Leznoff, A. B. P. Lever, *Phthalocyanines: Properties and Applications*, Vols I-IV, VCH, New York **1989–1996**.
- [9] H. Zollinger, *Color Chemistry: Synthesis, Properties, and Applications of Organic Dyes and Pigments*, 3rd ed., Verlag Helvetica Chimica Acta & Wiley-VCH, Zurich **2003**.
- [10] a) A. L. Thomas, *Phthalocyanine Research and Applications*, CRC Press, Boca Raton, FL **1990**. b) F. H. Thomas, A. L. Moser, *The Phthalocyanines*, Vol. 1, CRC Press, Boca Raton, FL **1983**.
- [11] a) S. I. Ogura, K. Tabata, K. Fukushima, T. Kamachi, I. Okura, *J. Porphyrins Phthalocyanines* **2006**, *10*, 1116; b) E. A. Lukyanets, *J. Porphyrins Phthalocyanines* **1999**, *3*, 424; c) C. M. Allen, W. M. Sharman, J. E. Van Lier, *J. Porphyrins Phthalocyanines* **2001**, *5*, 161; d) J. Y. Liu, X. J. Jiang, W. P. Fong, D. K. P. Ng, *Org. Biomol. Chem.* **2008**, *6*, 4560.
- [12] N. B. McKeown, *Phthalocyanine Materials: Synthesis, Structure and Function*, Cambridge University Press, Cambridge **1998**.
- [13] M. Wyler, US Patent 2197458, **1940**.
- [14] a) J. W. Steed, D. R. Turner, K. Wallace, *Core Concepts in Supramolecular Chemistry and Nanochemistry*, John Wiley, Chichester **2007** 37; b) D. K. MacFarland, C. M. Hardin, M. J. Lowe, *J. Chem. Educ.* **2000**, *77*, 1484; c) H. Z. Gök, H. Kantekin, Y. Gök, G. Herman, *Dyes Pigm.* **2007**, *75*, 606; d) M. N. Kopylovich, V. Y. Kukushkin, M. Haukka, K. V. Luzyanin, A. J. L. Pombeiro, *J. Am. Chem. Soc.* **2004**, *126*, 15040.
- [15] W. J. Youngblood, *J. Org. Chem.* **2006**, *71*, 3345.
- [16] a) H. Tomoda, S. Saito, S. Shiraishi, *Chem. Lett.* **1983**, *3*, 313; b) D. Wöhrle, G. Schnurpfeil, G. Knothe, *Dyes Pigm.* **1992**, *18*, 91; c) C. H. Lee, D. K. P. Ng, *Tetrahedron Lett.* **2002**, *43*, 4211; d) S. M. S. Chauhan, S. Agarwal, P. Kumari, *Synth. Commun.* **2007**, *37*, 2917; e) W. Liu, C. H. Lee, H.-W. Li, C. K. Lam, J. Wang, T. C. W. Mak, D. K. P. Ng, *Chem. Commun.* **2002**, 628; f) I. Özçesmeçi, A. I. Okur, A. Gül, *Dyes Pigm.* **2007**, *75*, 761.
- [17] T. D. Smith, J. Livorness, H. Taylor, J. R. Pilbrow, G. R. Sinclair, *J. Chem. Soc. Dalton Trans.* **1983**, 1391.
- [18] R. P. Linstead, E. G. Noble, J. M. Wright, *J. Chem. Soc.* **1937**, 911.
- [19] F. H. Moser, A. L. Thomas, *Phthalocyanines*, ACS Monograph 157, Reinhold Publishing, New York **1963**.

- [20] L. J. Boucher, in *Coordination Chemistry of Macrocyclic Compounds*, (Ed: G. A. Melson), Plenum Press, New York **1979**, 461.
- [21] L. F. Lindoy, D. H. Busch, in *Preparative Inorganic Reactions*, (Ed: W. L. Jolly), Wiley-Interscience, New York **1971**.
- [22] A. H. Jackson, in *The Porphyrins I (Structure and Synthesis. Part A)*, (Ed: D. Dolphin), Academic Press, New York **1978**, 365.
- [23] N. Fukada, *Nippon Kagaku Zasshi* **1957**, *78*, 1348 (*Cheni. Abs.* 1959, *53*, 12339b).
- [24] M. Yokote, F. Shibamiya, *Kogyo Kagaku Zudii* **1958**, *61*, 994 (*Chem. Ah.* 1961, *55*, 187698).
- [25] a) M. Yokote, F. Shibamiya, S. Tokairin, *Kogyo Kagaku Zasshi* **1964**, *67*, 166 (*Chem. Abs.* 1964, *61*, 3235f); b) J. E. Scott, *Histochemie* **1972**, *32*, 191; c) E. G. Gal'pern, E. A. Lukyanets, M. G. Galpern, *Izo. Akad. Nauk SSSR Ser. Khim.* **1973**, *9*, 1976; d) J. Alzeer, P. J. C. Roth, N. W. Luedtke, *Chem. Commun.* **1970**, 2009.
- [26] M. Yokote, F. Shibamiya, H. Yokornizao, *Yuki Gosei Kagaku Kyokai Shi* **1969a**, *27*, 340 (*Chem. Abs.* 1969, *71*, 38931h).
- [27] M. Yokote, F. Shibamiya, N. Sakikubo, *Yuki Gosei Kagaku Kyokai Shi* **1969b**, *27*, 448 (*Chem. Abs.* 1969, *72*, 125956p).
- [28] M. Yokote, F. Shibamiya, *Kogyo Kagaku Zasshi* **1959**, *62*, 720 (*Chem. Ah.* 1962, *57*, 9856c).
- [29] M. G. Galpern, E. A. Lukyanets, *Zh. Obshch. Khim.* **1969**, *39*, 2536.
- [30] a) A. Strecker, *Ann. Chem. Pharm.* **1850**, *75*, 27; b) M. B. Smith, J. March, *March's Advanced Organic Chemistry: Reactions, Mechanisms, and Structure*, 5th ed., Wiley-Interscience, New York **2001** 1240; c) A. R. Moosavi-Zare, M. A. Zolfigol, S. Farahmand, A. Zare, A. R. Pourali, R. Ayazi-Nasrabadi, *Synlett* **2014a**, *25*, 193; d) M. A. Zolfigol, A. Khazaei, A. R. Moosavi-Zare, A. Zare, V. Khakyzadeh, *Appl. Catal. A* **2011**, *400*, 70; e) A. R. Moosavi-Zare, M. A. Zolfigol, M. Daraei, *Synlett* **2014b**, *25*, 1173; f) A. R. Moosavi-Zare, M. A. Zolfigol, Z. Rezanejad, *Can. J. Chem.* **2016a**, *94*, 626; g) A. R. Moosavi-Zare, M. A. Zolfigol, R. Salehi-Moratab, E. Noroozizadeh, *J. Mol. Catal. A* **2016b**, *415*, 144; h) A. R. Moosavi-Zare, M. A. Zolfigol, O. Khaledian, V. Khakyzadeh, M. Darestani Farahani, H. G. Kruger, *New J. Chem.* **2014c**, *38*, 2342; i) A. R. Moosavi-Zare, M. A. Zolfigol, O. Khaledian, V. Khakyzadeh, M. Darestani farahani, M. H. Beyzavi, H. G. Kruger, *Chem. Eng. J.* **2014d**, *248*, 122.
- [31] D. Enders, J. P. Shilvock, *Chem. Soc. Rev.* **2000**, *29*, 359.
- [32] T. Vilaivan, C. Winotapan, T. Shinada, Y. Ohfune, *Tetrahedron Lett.* **2001**, *42*, 9073.
- [33] T. Vilaivan, C. Winotapan, V. Banphavichit, T. Shinada, Y. Ohfune, *J. Org. Chem.* **2005**, *70*, 3464.
- [34] C.-L. K. Lee, H. Y. Ling, T.-P. Loh, *J. Org. Chem.* **2004**, *69*, 7787.
- [35] B. Molle, P. Bauer, *J. Am. Chem. Soc.* **1982**, *104*, 3481.
- [36] S. K. De, R. A. Gibbs, *Tetrahedron Lett.* **2004**, *45*, 7407.
- [37] J. S. Yadav, B. V. Subba Reddy, B. Eeshwaraiiah, M. Srinivas, *Tetrahedron* **2004**, *60*, 1767.
- [38] L. Royer, S. K. De, R. A. Gibbs, *Tetrahedron Lett.* **2005**, *46*, 4595.
- [39] R. Martínez, D. J. Ramón, M. Yus, *Tetrahedron Lett.* **2005**, *46*, 8471.
- [40] A. S. Paraskar, A. Sudalai, *Tetrahedron Lett.* **2006**, *47*, 5759.
- [41] B. Das, R. Ramu, B. Ravikanth, K. R. Reddy, *Synthesis* **2006**, 1419.
- [42] a) S. Harusawa, Y. Hamada, T. Shioiri, *Tetrahedron Lett.* **1979**, *20*, 4663; b) K. Mai, G. Patil, *Tetrahedron Lett.* **1984**, *25*, 4583. c) S. Kobayashi, H. Ishitani, *Chem. Rev.* **1999**, *99*, 1069.
- [43] A. Heydari, P. Fatemi, A.-A. Alizadeh, *Tetrahedron Lett.* **1998**, *39*, 3049.
- [44] S. K. De, R. A. Gibbs, *J. Mol. Catal. A* **2005**, *232*, 123.
- [45] a) B. A. Horenstein, K. Nakanishi, *J. Am. Chem. Soc.* **1989**, *111*, 6242; b) J. Mulzer, A. Meier, J. Buschmann, P. Luger, *Synthesis* **1996**, 123.
- [46] H. A. Oskooie, M. M. Heravi, K. Bakhtiari, V. Zadsirjan, F. F. Bamoharram, *Synlett* **2006**, 1768.
- [47] B. C. Ranu, S. S. Dey, A. Hajra, *Tetrahedron* **2002**, *58*, 2529.
- [48] a) M. Safaiee, M. A. Zolfigol, F. Afsharnadery, S. Baghery, *RSC Adv.* **2015**, *5*, 102340; b) M. A. Zolfigol, M. Safaiee, N. Bahrami-Nejad, *New J. Chem.* **2016**, *40*, 5071; c) M. A. Zolfigol, S. Baghery, A. R. Moosavi-Zare, S. M. Vahdat, *RSC Adv.* **2015a**, *5*, 32933; d) M. A. Zolfigol, S. Baghery, A. R. Moosavi-Zare, S. M. Vahdat, H. Alinezhad, M. Norouzi, *RSC Adv.* **2015b**, *5*, 45027.
- [49] M. G. Dekamin, M. Azimoshan, L. Ramezani, *Green Chem.* **2013**, *15*, 811.
- [50] A. R. Hajipour, Y. Ghayeb, N. Sheikhan, *J. Iran. Chem. Soc.* **2010**, *7*, 447.
- [51] M. G. Dekamin, Z. Karimi, M. Farahmand, *Catal. Sci. Technol.* **2012**, *2*, 1375.
- [52] A. R. Hajipour, I. Mahboobi Dehbane, *Iran. J. Catal.* **2012**, *2*, 147.
- [53] G. K. S. Prakash, T. E. Thomas, I. Bychinskaya, A. G. Prakash, C. Panja, H. Vaghoo, G. A. Olah, *Green Chem.* **2008**, *10*, 1105.
- [54] a) G. Hopfengärtner, D. Borgmann, I. Rademacher, G. Wedler, E. Hums, G. W. Spitznagel, *J. Electron Spectrosc. Relat. Phenom.* **1993**, *63*, 91; b) B. F. Dzhurinskii, D. Gati, N. P. Sergushin, V. I. Nefedov, Y. V. Salyn, *Russ. J. Inorg. Chem.* **1975**, *20*, 2307.
- [55] M. G. Dekamin, S. Sagheb-Asl, M. R. Naimi-Jamal, *Tetrahedron Lett.* **2009**, *50*, 4063.
- [56] M. G. Dekamin, Z. Mokhtari, Z. Karimi, *Sci. Iran. C* **2011**, *18*, 1356.

SUPPORTING INFORMATION

Additional Supporting Information may be found online in the supporting information tab for this article.

How to cite this article: Baghery S, Zolfigol MA, Safaiee M, Alonso DA, Khoshnood A. Novel nano molten salt tetra-2,3-pyridiniumporphyrinato-oxovanadium tricyanomethanide as a vanadium surface-free phthalocyanine catalyst: Application to Strecker synthesis of α -aminonitrile derivatives. *Appl Organometal Chem.* 2017;e3775. <https://doi.org/10.1002/aoc.3775>